J Mater Sci (2008) 43:4247–4256
DOI 10.1007/s10853-008-2615-0

Morphology and composition of nickel–boron nanolayer coating on boron carbide particles

Hongying Dong · Xiaojing Zhu · Kathy Lu

Received: 19 December 2007 / Accepted: 25 March 2008 / Published online: 9 April 2008

Abstract This work is focused on electroless coating of Ni–B nanolayer on B_4C particle surfaces. The B_4C particles used are approximately 2 μm in average size. Effects of activation agent $PdCl_2$, complexing agent $C_2H_8N_2$, and reducing agent $NaBH_4$ addition rate are studied. The solids loading of B_4C is 0.625 g/L and the concentration of Ni^{2+} ions is 0.004 mol/L in the electroless coating solution. Scanning electron microscopy (SEM) shows that when B_4C:Pd^{2+} molar ratio is 1:0.005, a Ni–B nanolayer with the smallest Ni–B nodule size covers the B_4C particle surfaces. Complexing agent $C_2H_8N_2$ decreases Ni^{2+} ion release rate. Ni:$C_2H_8N_2$ ratio of 1:6 is the preferred complexing agent amount for achieving a continuous Ni–B nanolayer. The Ni–B nanolayer formation is also strongly dependent on the rate that Ni^{2+} ions are reduced. Slow Ni^{2+} reduction leads to increased Ni content in the Ni–B nanolayer. When the above three factors are combined at the optimal values for the electroless coating process, well-defined Ni–B nanolayer is obtained. SEM cross section analysis shows the Ni–B nanolayer completely covers the B_4C particles with less than 55 nm thickness.

Introduction

B_4C is the third hardest material known (hardness 2,900–3,900 kg/mm^2), ranking after diamond (8,000–8,500 kg/mm^2) and cubic boron nitride (4,500–4,600 kg/mm^2) [1]. Besides the hardness, its unique properties, such as good chemical resistance, low density (2.52 g/cm^3), and neutron absorption properties, make B_4C an important material in different applications. B_4C can be used for dressing diamond tools, hot-pressed shot blast nozzles, ceramic tooling dies, and armors [2, 3]. B_4C is also used as an absorbent for neutron radiation in nuclear power plants in the form of shielding, control rod, and shut down pellets [4]. In spite of these very attractive properties, achieving high-density B_4C components has been a challenge. B_4C particles are extremely hard and do not deform under typical compaction pressure. Also, B_4C is difficult to sinter because of the low boron and carbon diffusion mobility resulting from covalent bonding. If a metallic layer can be incorporated into the B_4C system, it should greatly facilitate the re-arrangement of the B_4C particles during compaction and the diffusion of the B_4C species during sintering. When the metallic layer is controlled at a very low amount and distributed homogeneously around the B_4C particles, mechanical property degradation should be avoided and new functionalities such as electrical conductivity and magnetism can possibly be introduced.

Several methods have been used to produce surface layer on particles, such as solution coating [5, 6], micelle-assisted coating [7], and heterocoagulation coating [8, 9]. However, these methods are exclusively developed for oxide or semiconductor type coating. Electroless coating presents as one of the few options coating thin metallic layer onto particles. The method is an autocatalytic reduction process of metallic ions onto surfaces in aqueous solutions with no electric current or voltage requirement. It has the advantage of coating the metallic layer uniformly on the surface of particles instead of producing a simple mixture of the two compositions. An electroless coating bath typically contains metal salt, reducing agent, complexing agent, and stabilizer.

H. Dong · X. Zhu · K. Lu (✉)
Department of Materials Science and Engineering, Virginia Polytechnic Institute and State University, 213 Holden Hall-M/C 0237, Blacksburg, VA 24061, USA
e-mail: klu@vt.edu

Since no current is used, the reaction rate can be controlled and adjusted more easily. The process is traditionally used to coat metallic layers onto substrates [10–14]. In recent years, it is being increasingly used to coat metallic layers onto particles, fibers, or even tubes. For example, nickel was coated onto carbon fibers, but the coating was thick and rough and the process substantially increased carbon fiber diameters [15]. Palladium was coated onto carbon nanotubes but was in particle format to 'decorate' the carbon nanotubes [16]. For nickel–phosphorous electroless coating onto carbon nanotubes, similar nanoparticle morphology was observed [17]. Nickel was also coated onto SiC particles by electroless coating, but the coating morphology was not discussed [18]. When Ni–B layer was coated onto WC and VC powders [19], continuous Ni-rich layer was obtained, but the coated particles severely agglomerated.

With continuing interest in designing and modifying particle surfaces for processing and performance improvement, electroless coating process needs to be re-examined, especially on the coating morphology and composition. In our prior work [20], electroless coating of Ni–B nanolayer onto B_4C particles was studied. The Ni–B nanolayer by definition means full coverage of B_4C particle surfaces with a less than 100 nm thickness layer. Using $NiSO_4$ as a Ni^{2+} source, $SnCl_2$ as a sensitizing agent, $PdCl_2$ as an activation agent, and $NaBH_4$ as a reducing agent, Ni–B nanolayers of different thicknesses were successfully coated onto B_4C particles. The Ni–B nanolayer thickness can be adjusted by Ni^{2+}:B_4C molar ratio. With the Ni–B nanolayer thickness increase, Ni–B nodules appear in-between the mesh-like, seemingly porous Ni–B nanolayer structures and the nodule size grows with the nanolayer thickness. Energy dispersive spectroscopy (EDS) and X-ray photoelectron spectroscopy (XPS) results show the presence of oxygen in the Ni–B nanolayer as Ni_2O_3 and B_2O_3. Ni:B ratio in the Ni–B nanolayer decreases with the layer thickness. Fundamental Ni–B electroless coating processes and morphological changes on the B_4C particle surfaces with different layer thickness have also been analyzed.

Based on the knowledge obtained from the previous study [20], this work is focused on understanding the effects of activation agent $PdCl_2$, complexing agent $C_2H_8N_2$, and reducing agent $NaBH_4$ addition rate on the Ni–B nanolayer morphology and composition. The optimal condition for each factor is evaluated to obtain uniform and continuous Ni–B nanolayer. Under the optimal electroless coating conditions for all the three factors, scanning electron microscopy (SEM) cross section analysis is conducted to analyze the Ni–B nanolayer morphology and thickness. It has been observed that the Ni–B nanolayer completely covers every B_4C particle surface and the Ni–B nanolayer composition can be varied.

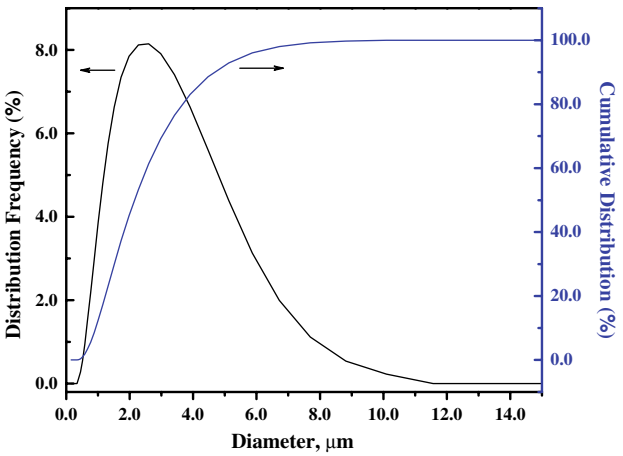

Fig. 1 Size distribution of B_4C particles used in this study

Experimental procedure

Figure 1 shows the size distribution of the B_4C particles used (H. C. Starck, Inc., Newton, MA). There were three runs for the particle size distribution analysis. The particles have 8.3 m^2/g specific surface area (Quantachrome ASIC VP7 Surface Area Analyzer, Boynton Beach, FL) and 2.27 μm average particle size (Horiba, LA-950, Irvine, CA). The particle size distribution is volume based. D_{10}, D_{50}, and D_{90} are 0.92, 2.15, and 4.67 μm, respectively. Figure 2 is the SEM image of the B_4C particles used in this study.

Before the electroless coating process was carried out, the B_4C particles were sensitized using $SnCl_2$ and activated using $PdCl_2$. The surface sensitization was carried out by adding B_4C particles into $SnCl_2 \cdot 2H_2O$ (>98%, Fisher Scientific, Fair Lawn, NJ) and HCl (36–38%, EMD, Gibbstown, NJ) solution (0.07 M $SnCl_2 \cdot 2H_2O$, 40 mL/L HCl). The suspension was sonicated for 10 min at room temperature. The Sn^{2+} sensitized B_4C particles were thoroughly washed and

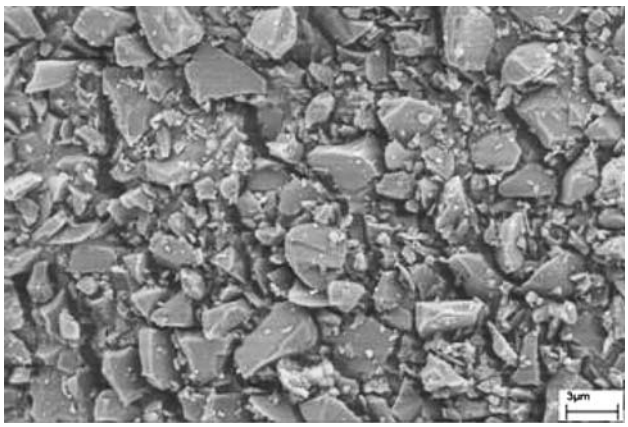

Fig. 2 SEM image of B_4C particles used in this study

transferred to a $PdCl_2$ (>99%, Fisher Scientific, Fair Lawn, NJ) and HCl solution (0.0042 M $PdCl_2$, 40 mL/L HCl) for activation. After sonication for another 10 min in the activating solution, the activated B_4C particles were again thoroughly washed with de-ionized water and then introduced into the electroless coating bath. $NiSO_4 \cdot 6H_2O$ (99.0%, Fisher Scientific, Fair Lawn, NJ) was used as the Ni^{2+} source at 0.004 mol/L concentration. Ni^{2+} was complexed to avoid $Ni(OH)_2$ formation and the complexing agent used in this work was ethylenediamine ($C_2H_8N_2$, Fisher Scientific, Fair Lawn, NJ). The solids loading of B_4C in the electroless coating solution was 0.625 g/L. The Ni:B_4C molar ratio was 0.3354. Reducing agent $NaBH_4$ (Fisher Scientific, Fair Lawn, NJ) was introduced into the complexed Ni^{2+} solution. The electroless coating was carried out at 85 ± 2°C. The electroless coating time was 30 min and mechanical stirring was provided by plastic stirring blades. The pH value of the coating bath was adjusted with NaOH (Fisher Scientific, Fair Lawn, NJ) to 12–14. The electroless coating process was then carried out by adding $NaBH_4$ into the electroless coating bath. Since the reduction time was short and $NaBH_4$ decomposition was not a problem, no stabilizer was used in this study. The chemical compositions and the electroless coating conditions are listed in Table 1.

A field emission SEM equipped with an EDS (LEO 1550, Carl Zeiss MicroImaging, Inc., Thornwood, NY) was used to characterize the surface morphology of the Ni–B nanolayers. XPS (Perkin Elmer 5400, Minneapolis, MN) was employed to characterize the composition of the Ni–B nanolayers. A dual beam focused ion beam microscope (FIB) (Helios NanoLab, FEI Co., Hillsboro, OR) was used to cross-section the Ni–B coated B_4C particles for the nanolayer thickness and morphology analyses. Both SEM and FIB samples were prepared as follows. Dry B_4C or Ni–B nanolayer coated B_4C particles were attached onto one side of a double-sided conductive carbon tape, while the other side of the tape was attached onto a SEM sample holder. An air duster was used to spray off any particles loosely attached to the carbon tape. Before the sample was put into the SEM or FIB chamber, the attached particles were coated with 10 nm gold using a sputter coater (208HR, Cressington Scientific Instruments Ltd., Watford, England) to ensure the conductivity of the samples. The as-is B_4C particles and the Ni–B nanolayer coated B_4C particles were directly imaged by SEM. Also, the Ni–B nanolayer coated B_4C particles were cross-sectioned by the FIB. The Ni–B nanolayer thickness was measured from the cross section images of the B_4C particles using the dimensional measurement feature on the FIB. The imaging resolution was 1.5 nm.

Results and discussion

Activation agent effect

According to the mechanism analysis of the Ni–B nanolayer formation in our prior work [20], Pd^{2+} oxidizes Sn^{2+} to Sn^{4+} and converts itself into Pd^0 on the B_4C surfaces during the activation step. Pd^0 atoms act as catalytic centers in the initial stage of the electroless coating of the B_4C particle surfaces. The reduced Ni species then acts as the autocatalytic centers for further Ni^{2+} reduction. Based on the atomic radius of Pd^0 and the specific surface area of B_4C particles, each Pd^0 atom will cover about 10^{-19} m^2 surface area of B_4C particles. For a monolayer Pd^0 surface coverage on B_4C particles, this corresponds to B_4C:Pd^{2+} molar ratio of 1:0.01. Our prior work of 1:0.04 B_4C:Pd^{2+} ratio indicated that Pd^{2+} is excessive, consistent with the study by Brandow et al. [21]. To evaluate the B_4C:Pd^{2+} ratio effect on the Ni–B nanolayer morphology, B_4C:Pd^{2+} molar ratios of 1:0.04, 1:0.01, 1:0.005, and 1:0.001 were studied at Ni:$C_2H_8N_2$ ratio of 1:6 and $NaHB_4$ addition rate of 10 drops/min.

Figure 3 shows the SEM images of the as-is B_4C particle surface and the surface of the B_4C particles coated with Ni–B nanolayers using different amounts of $PdCl_2$ for B_4C particle surface activation. When the B_4C:Pd^{2+} molar ratio is 1:0.04 (four times of Pd^0 needed for monolayer coverage on the B_4C surfaces), rough coating layer with large Ni–B nodules (bright spots) is observed. When the B_4C:Pd^{2+} ratio is decreased to 1:0.01 (Pd^0 monolayer coverage on the B_4C surfaces), coating roughness remains almost the same. Mesh-like and porous nanostructures among the Ni–B nodules can be observed. This means high $PdCl_2$ amount can over activate the B_4C particle surfaces and cause the Ni–B nanolayer to grow too fast. Since ideal monolayer Pd^0 packing on the B_4C surfaces is unlikely,

Table 1 Chemical compositions of electroless coating bath

Ni:B_4C (molar ratio)	B_4C:Sn^{2+} (molar ratio)	Ni:$NaBH_4$ (molar ratio)	B_4C:Pd^{2+} (molar ratio)	Ni:$C_2H_8N_2$ (molar ratio)	$NaBH_4$ addition rate
0.3354	01:0.7	1:1	1:0.04	1:4.5	All in one time
			1:0.01	1:6	10 drops/min
			1:0.005	1:9	1 drop/min
			1:0.001		

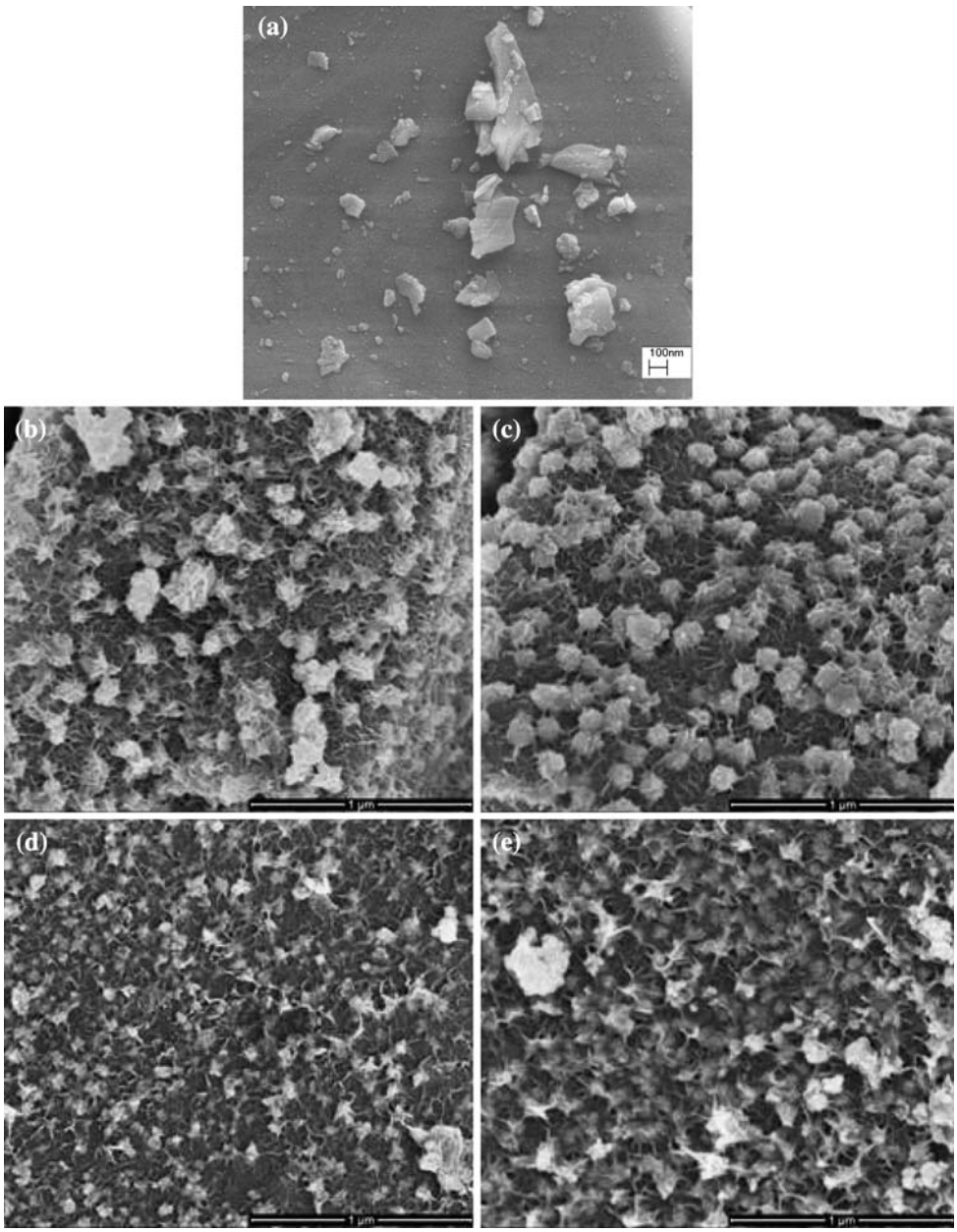

Fig. 3 SEM images of initial B_4C particle surface and Ni–B nanolayers on B_4C particles obtained under different molar ratios of B_4C:Pd^{2+}: (**a**) initial B_4C particle surface, (**b**) 1:0.04 B_4C:Pd^{2+} molar ratio, (**c**) 1:0.01 B_4C:Pd^{2+} molar ratio, (**d**) 1:0.005 B_4C:Pd^{2+} molar ratio, and (**e**) 1:0.001 B_4C:Pd^{2+} molar ratio

some Pd^0 atoms may exist as clusters at certain locations. As a result, the Ni–B nodules quickly form at the Pd^0 cluster locations and act as the initiation sites for nodule growth. If the electroless coating process continues under such condition, particles will form on the to-be-coated surfaces, as seen in other studies [15–18]. When the B_4C:Pd^{2+} molar ratio is decreased to 1:0.005, Ni–B coating with much smaller Ni–B nodules is obtained. This means fewer activation sites on the B_4C particles are more conducive for the Ni–B nanolayer formation while suppressing excessive Ni–B nodule growth. For the studied B_4C particles, the Pd^0 concentration on the particles should be half of the Pd^0 monolayer surface coverage. With further B_4C:Pd^{2+} molar ratio decrease to 1:0.001, the Ni–B nanolayer becomes rough again and the size of the Ni–B nodules increases, even though much smaller than those of the first two B_4C:Pd^{2+} ratios. This surface roughening is likely because the Pd^0 activated sites are too far apart (under-activated), the diffusion distances needed for the newly reduced Ni and B species to reach the growing nanolayer edge are too long. When the newly reduced Ni and B species continuously deposit on the Ni–B nanolayer itself at proximate locations, Ni–B nodules form but in a more mesh-like morphology than that formed under

over-activated conditions. As shown in Fig. 3d, the under-activated B_4C particle surface shows rough but more homogeneous Ni–B nanolayer; B_4C:Pd^{2+} ratio of 1:0.005 shows to be the optimal activation condition.

The Ni–B nanolayer morphologies obtained using different amounts of activation agent $PdCl_2$ show that there is an optimal Pd^0 surface concentration to achieve desired nanolayer and avoid particle formation on the coating surface. Pd^0 concentration affects the Ni–B nanolayer growth initiation sites, the Ni–B deposition rate, and subsequently the Ni–B nanolayer morphology. When too much $PdCl_2$ is used for B_4C surface activation, Ni and B species attach to the B_4C surfaces at a high rate. However, the nanolayer growth mode requires that the Ni and B species diffuse to the growing layer edge. Since some Ni and B species do not have enough time to diffuse long distance and attach to the growing layer edge before the arrival of more reduced species, these newly reduced species will deposit on top of the prior Ni–B deposit layer. This leads to localized nodule growth. When too little $PdCl_2$ is used for B_4C particle surface activation, the diffusion distance to the growing nanolayer edge is too long and the reduced species will deposit 'middle-way,' again forming rougher Ni–B nanolayers, as seen in Fig. 3.

It should be pointed out that Fig. 3 only reveals the Ni–B nanolayer morphology. The Ni–B nanolayer composition serves as another important aspect in evaluating the effect of the activation agent $PdCl_2$ amount. Figure 4 shows the XPS spectra of the original B_4C particles and the Ni–B nanolayer coated B_4C particles obtained with different amounts of activation agent $PdCl_2$. For all B_4C:Pd^{2+} molar ratios, B–O bond peak dominates the XPS spectra.

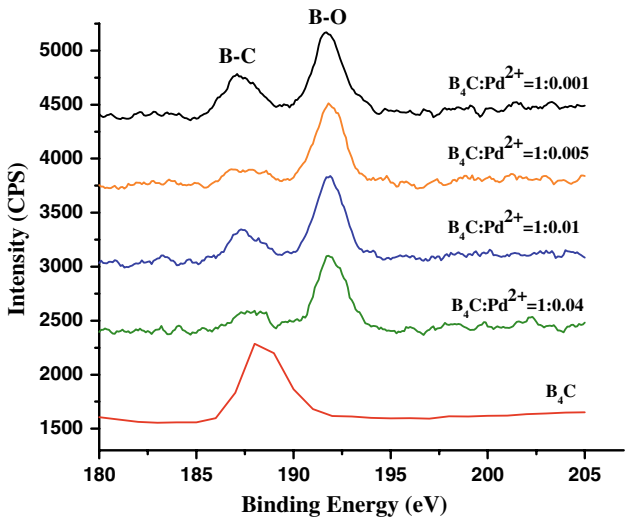

Fig. 4 XPS spectra of as-is B_4C particles and B_4C particles coated with Ni–B nanolayers from different molar ratios of B_4C:Pd^{2+}

As discussed before [20], B_2O_3 forms during the Ni–B nanolayer formation process. The existence of the B–O bond peak means that the B_4C particles are mostly covered with the Ni–B nanolayer. The difference among the spectra is mainly on B–C bond peak. When the B_4C:Pd^{2+} ratio is 1:0.005, the intensity of the B–C bond peak is the lowest; very weak B–C bond peak from the B_4C particle surfaces is detected. This means B_4C:Pd^{2+} ratio of 1:0.005 offers the best Ni–B nanolayer surface coverage of the B_4C particles. At the other three B_4C:Pd^{2+} ratios, the Ni–B nanolayer surface coverage of the B_4C particles is less defined. The B–C bond peak can be easily detected, likely due to the uneven Ni–B nanolayer morphology on the B_4C particle surfaces, with some locations being thinner and some locations being thicker than the XPS detection depth. Even though the porosity of the Ni–B nanolayer cannot be measured, the rough appearance of the Ni–B nanolayers are consistent with the XPS results, indicating that B_4C:Pd^{2+} ratio of 1:0.005 offers Ni–B nanolayer of more uniform thickness and is the optimal $PdCl_2$ content for the B_4C particle surface activation.

Complexing agent effect

Ni^{2+} ions in aqueous solution do not stay as free ions. Instead, they are bound to a specific number of water molecules in the form of $[Ni(H_2O)_x]^{2+}$ ($x = 1$–6). To avoid $Ni(OH)_2$ formation under alkaline condition, Ni^{2+} ions must be complexed with a stronger complexing agent than water before being exposed to high pH conditions during the electroless coating process. In this study, the complexing agent is $C_2H_8N_2$ and it plays three functions: preventing the pH of the solution from decreasing too fast, preventing the precipitation of $Ni(OH)_2$, and reducing the concentration of free Ni^{2+} ions. As shown in the structural Eq. 1, two of the six water molecules initially complexed with Ni^{2+} ions can be replaced by one $C_2H_8N_2$ molecule, forming type I nickel complex. Likewise, two or three $C_2H_8N_2$ molecules can complex with Ni^{2+} ions when four or six water molecules are replaced, forming type II and type III nickel complexes. The extent of complexing can be observed from the solution color change from blue to bright purple when $C_2H_8N_2$ is added. The most stable complex product is type III nickel complex and the theoretical molar ratio of Ni^{2+}:$C_2H_8N_2$ is 1:3. However, our experiments have shown that Ni^{2+}:$C_2H_8N_2$ ratio of 1:3 cannot stabilize Ni^{2+} ions. $Ni(OH)_2$ precipitate forms at pH 12–14 conditions. More $C_2H_8N_2$ than the above ratio is needed. In this work, Ni^{2+}:$C_2H_8N_2$ molar ratios of 1:4.5, 1:6, and 1:9 are studied to evaluate the effect of the complexing agent $C_2H_8N_2$. The B_4C:Pd^{2+} ratio is 0.04 and the $NaBH_4$ addition rate is 10 drops/min.

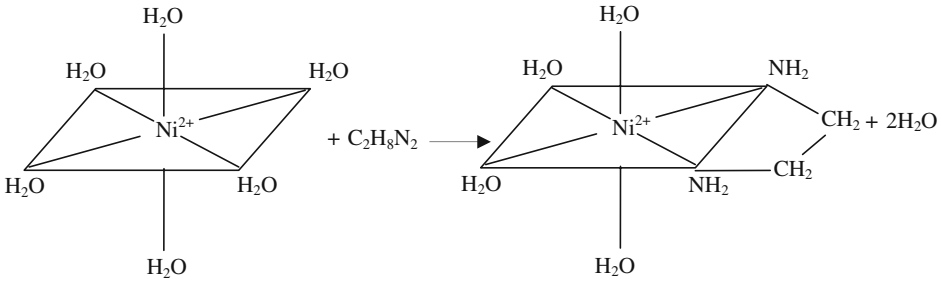

(1)

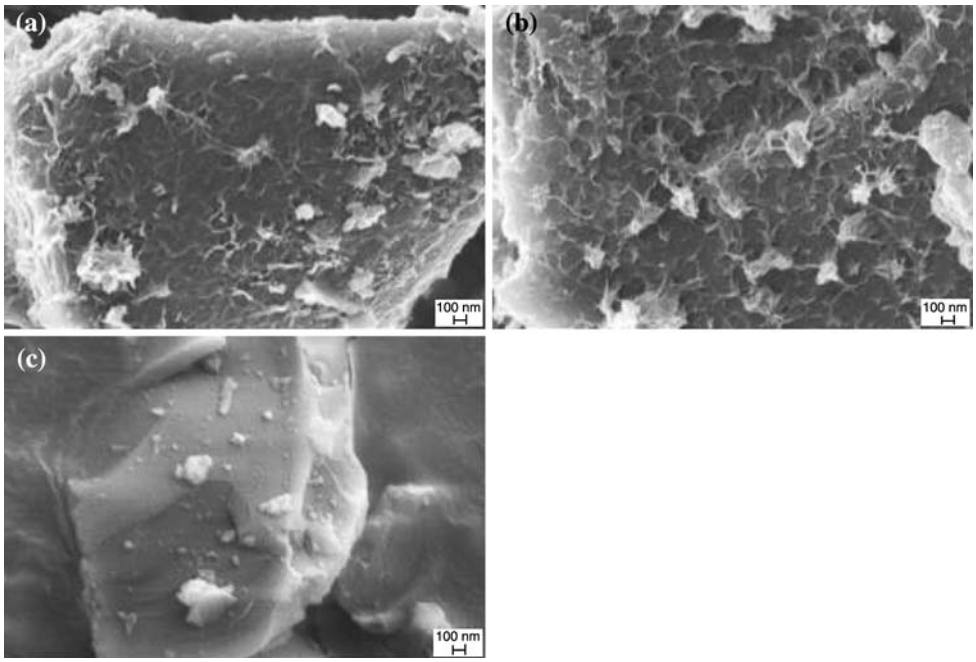

Fig. 5 SEM images of B_4C particles coated with Ni–B nanolayers from different Ni:$C_2H_8N_2$ ratios: (**a**) 1:4.5, (**b**) 1:6, and (**c**) 1:9

As shown in Fig. 5, when Ni^{2+}:$C_2H_8N_2$ ratio is 1:4.5, mesh-like layer covers the B_4C particle surfaces and Ni–B nodules can be observed (brighter spots). When Ni^{2+}:$C_2H_8N_2$ ratio is 1:6, the mesh-like morphology of the Ni–B nanolayer on the B_4C particle surfaces diminishes to more even surface, still with Ni–B nodules. When Ni^{2+}:$C_2H_8N_2$ ratio is 1:9, the B_4C particle surface is smooth and the sharp edges of the B_4C particles can be observed. This means increased Ni^{2+} ion stability and gradual Ni^{2+} ion release due to stronger complexing from $C_2H_8N_2$ are beneficial for more uniform Ni–B nanolayer formation. However, when Ni^{2+} is complexed too strongly to $C_2H_8N_2$, Ni^{2+} release into the electroless coating solution is substantially hindered and the Ni–B nanolayer formation rate becomes very slow (Fig. 5c), even though the chemical ratios of the electroless coating reactions remain the same.

Figure 6 shows the XPS spectra of the Ni–B coated B_4C particles with different Ni:$C_2H_8N_2$ ratios. When Ni^{2+}:$C_2H_8N_2$ ratio is 1:4.5, Ni–Ni, Ni–O, B–O, and B–C bond peaks are all observed. This means the Ni–B nanolayer is present but not uniform on the B_4C particle surfaces. Some areas have thin Ni–B nanolayer thickness and the photoelectrons from the B_4C particles are detected. When Ni^{2+}:$C_2H_8N_2$ ratio is 1:6, all the peaks are still present but

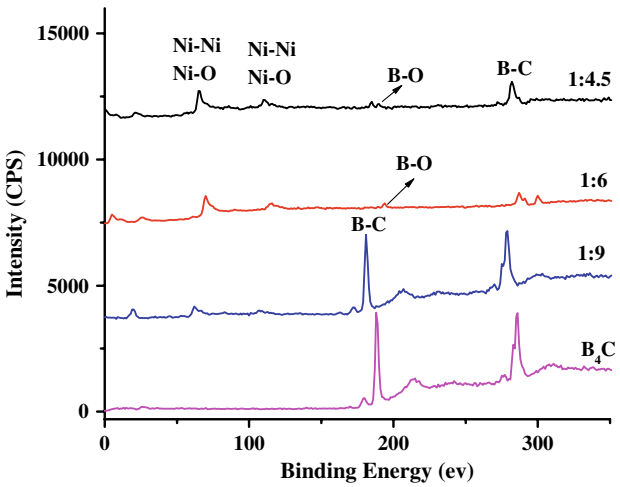

Fig. 6 XPS spectra of as-is B_4C particles and B_4C particles coated with Ni–B nanolayers using different $C_2H_8N_2$ amounts

the B–C bond peak is very low. This means the Ni–B nanolayer coverage on the B_4C particles is much improved. When Ni^{2+}:$C_2H_8N_2$ ratio is 1:9, however, strong B–C bond peak re-appears, similar to that of pure B_4C, while the Ni–Ni and Ni–O bond peaks are less defined. Combined with Fig. 5, this means the Ni–B nanolayer is too thin at Ni^{2+}:$C_2H_8N_2$ ratio of 1:9 and the XPS analysis detects the B–C bonds from the B_4C particles. Overall, modest Ni^{2+}:$C_2H_8N_2$ ratio facilitates the formation of the Ni–B nanolayer on the B_4C particle surfaces. Very low Ni^{2+}:$C_2H_8N_2$ ratio (excessive complexing agent) lowers the Ni^{2+} release rate to the electroless coating bath and results in very thin Ni–B nanolayer. Even though it is difficult to form stable Ni^{2+} complexes with low amount of complexing agent $C_2H_8N_2$, too much $C_2H_8N_2$ is also undesirable since it adversely affects Ni^{2+} availability for the Ni–B nanolayer formation. A balance needs to be achieved between the Ni–B nanolayer morphology and thickness. It is most desirable that the nanolayer have uniform thickness and homogeneous structure. Ni^{2+}:$C_2H_8N_2$ ratio of 1:6 is preferred in this work when both SEM and XPS results are considered.

Reduction rate effect

During the electroless coating process, reducing agent $NaBH_4$ reduces Ni^{2+} ions in $Ni(C_2H_8N_2)_x^{2+}$ to Ni. The Ni–B nanolayer formation is strongly dependent on the rate that Ni^{2+} can be reduced. Figure 7 shows the SEM images of the Ni–B coated B_4C particles with different $NaBH_4$ addition rate. The B_4C:Pd^{2+} ratio is 1:0.04 and the Ni:$C_2H_8N_2$ ratio is 1:6. When $NaBH_4$ is added into the electroless coating bath at one time, the Ni–B layer forms quickly and causes agglomeration of the B_4C particles (Fig. 7a). Multiple B_4C particles are encapsulated into a flaky cluster but some of the B_4C particle surfaces inside the cluster are not coated with the Ni–B nanolayer [22]. When the $NaBH_4$ addition rate is decreased to 10 drops/min (Fig. 7b), better defined Ni–B layer forms on the B_4C particle surfaces and the flaky morphology disappears. When the $NaBH_4$ addition rate is further reduced to 1 drop/min (Fig. 7c), thin and more uniform Ni–B layer with some bright nodules is observed.

Figure 8 shows the XPS spectra of the Ni–B coated B_4C particles with different $NaBH_4$ addition rate. When $NaBH_4$ is added at one time, the B–O bond peak dominates the XPS spectrum with a small B–C bond peak. This means the B_4C particle surfaces are mostly covered with the Ni–B nanolayer but some locations might have a very thin Ni–B layer. When $NaBH_4$ is added at 10 drops/min, the intensity of the B–O bond peak increases and that of the B–C bond peak slightly decreases. This means slower $NaBH_4$ addition rate is beneficial for improving the Ni–B nanolayer surface coverage on B_4C particles; more Ni and B are reduced and deposited on the B_4C particle surfaces. When $NaBH_4$ is added at 1 drop/min, the B–O bond peak is still present but the B–C bond peak dominates the XPS spectra. This is likely because the Ni–B nanolayer is too thin and the photo-electrons from the B_4C particles are detected, as reflected by the smooth surface shown in Fig. 7c.

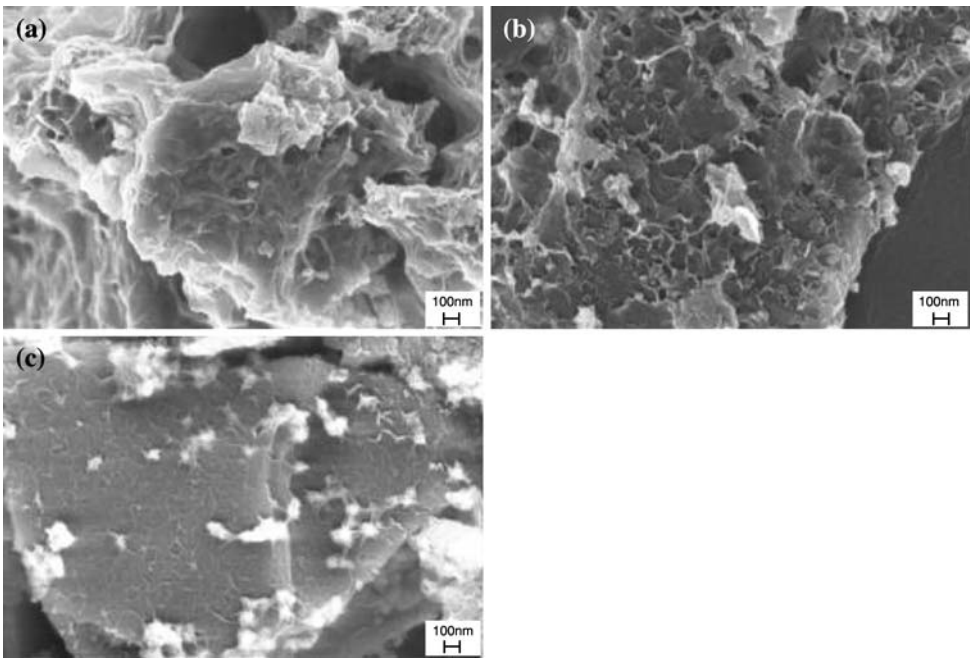

Fig. 7 SEM images of Ni–B nanolayers on B_4C particles obtained with different $NaBH_4$ addition rates: (**a**) all at one time, (**b**) 10 drops/min, and (**c**) 1 drop/min

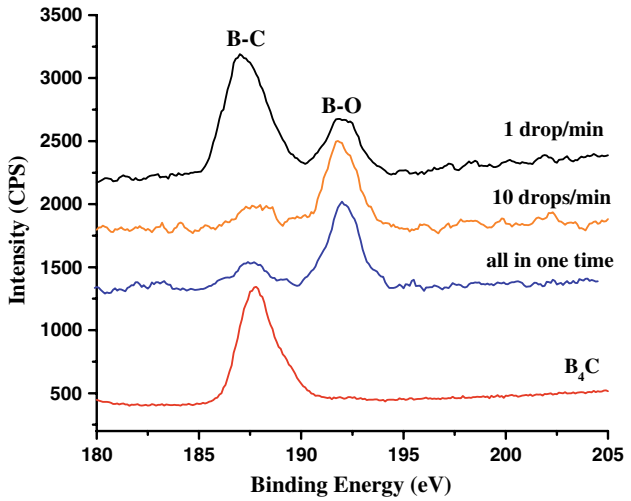

Fig. 8 XPS spectra of as-is B_4C particles and Ni–B nanolayer coated B_4C particles with different $NaBH_4$ addition rates

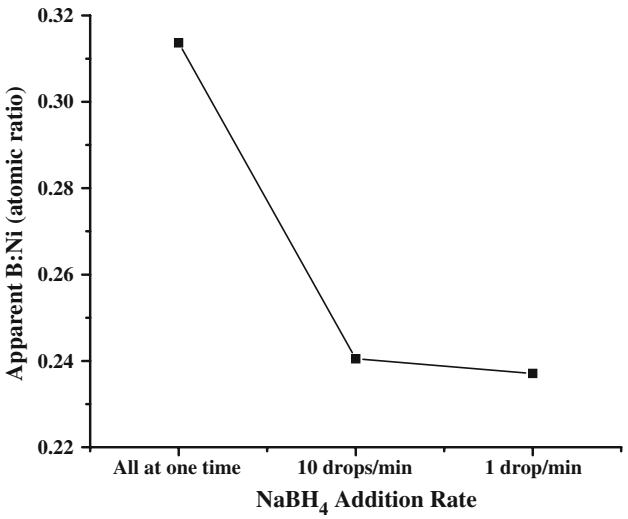

Fig. 9 Effect of $NaBH_4$ addition rate on apparent B:Ni atomic ratio in the Ni–B nanolayer

The effect of $NaBH_4$ addition rate can be further understood from the fundamentals of the electroless coating process. During the electroless coating, the following reactions occur [23]:

$$4Ni^{2+} + BH_4^- + 8OH^- \rightarrow 4Ni + BO_2^- + 6H_2O \quad (2)$$

$$BH_4^- + 4H_2O \rightarrow B(OH)_4^- + 4H_2 \uparrow \quad (3)$$

When the reducing agent $NaBH_4$ is added at a fast rate, BH_4^- is temporarily excessive. In addition to reaction with Ni^{2+}, BH_4^- can be oxidized to $B(OH)_4^-$, which can convert to B_2O_3 according to the following reactions:

$$B(OH)_4^- \rightarrow B(OH)_3 + OH^- \quad (4)$$

$$2B(OH)_3 \rightarrow B_2O_3 + 3H_2O \quad (5)$$

If this is the case, then the Ni–B nanolayer composition should change with the $NaBH_4$ addition rate, which directly influences the availability of BH_4^- on the B_4C particle surfaces. With faster $NaBH_4$ addition rate, BH_4^- species can be converted to B_2O_3 and the Ni content in the nanolayer should be low. To confirm such prediction, quantitative analysis of apparent B:Ni ratio in the Ni–B nanolayer was conducted. The percent of the peak area for a given bond in a given XPS spectra can be calculated based on:

$$X = \frac{\frac{I_x}{S_x T_x}}{\sum_1^n \frac{I_i}{S_i T_i}} \times 100 \quad (6)$$

n: number of XPS bond peaks examined, which is determined by the number and type of interested species. S_i: sensitivity factor, which is a constant for each chosen species. T_i: acquisition time per data point for a given species. I_i: XPS bond peak intensity of species i, which is calculated based on the peak height and area after background subtraction. The background is determined by drawing a straight line between the two endpoints of the XPS bond peak to be analyzed. At each data point the value of the background curve is subtracted from the value of the XPS spectrum curve. By comparing the percentage X of different interested species, a relative atomic ratio is obtained.

The results in Fig. 9 from quantitative XPS analysis indicate that indeed the Ni–B nanolayer composition varies with the $NaBH_4$ addition rate. When $NaBH_4$ is added at one time, the B:Ni ratio (only the B in the Ni–B nanolayer) is 0.314. When $NaBH_4$ is added at 10 drops/min, the B:Ni ratio is 0.240. When $NaBH_4$ is added at 1 drop/min, the B:Ni ratio is 0.237. To obtain uniform and continuous Ni–B nanolayer on the B_4C particles, $NaBH_4$ addition rate needs to be optimized with the consideration of the B:Ni ratio in the Ni–B nanolayer. In this study, very slow $NaBH_4$ addition rate (1 drop/min) does not affect the B–Ni ratio in the Ni–B nanolayer to an observable degree in comparison to the $NaBH_4$ addition rate of 10 drops/min as shown in Fig. 9. This means $NaBH_4$ addition rate of 10 drops/min does not create excessive BH_4^- ions. Also, $NaBH_4$ addition rate of 1 drop/min is too slow to be practical. In this and future studies, $NaBH_4$ addition rate of 10 drops/min is used.

Optimized Ni–B nanolayer

Based on the results obtained from activation agent $PdCl_2$, complexing agent $C_2H_8N_2$, and reducing agent $NaBH_4$ addition rate, the respective optimal condition for each factor is: B_4C:Pd^{2+} molar ratio at 1:0.005, Ni:$C_2H_8N_2$ ratio

at 1:6, and $NaBH_4$ addition rate at 10 drops/min. As a combinational step of obtaining optimal Ni–B nanolayer on B_4C particle surfaces, electroless coating process is carried out under the conditions optimized individually for each factor. Figure 10 shows the Ni–B nanolayer obtained at low and high magnifications. In comparison to the preferred nanolayer morphology under separate conditions (Figs. 3d, 5b, and 7b), Fig. 10 shows full Ni–B nanolayer coverage on every B_4C particles and the nanolayer has the fewest number of Ni–B nodules and the least obvious mesh structures.

Figure 11 shows the cross section SEM image of the B_4C particles with optimized Ni–B nanolayer coating. The bright Ni–B nanolayers uniformly distribute around all the darker color B_4C particle surfaces as shown at the bottom half of the image. The top half of the image shows a single

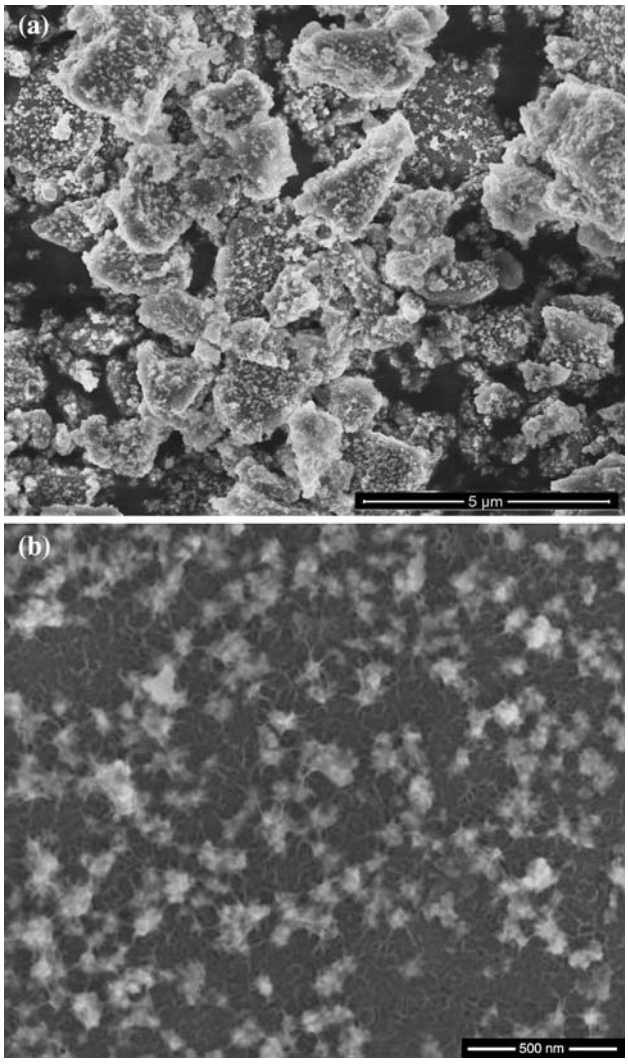

Fig. 10 SEM micrograph of Ni–B nanolayer on B_4C particles with all three conditions at the optimal values: (**a**) low magnification, (**b**) high magnification

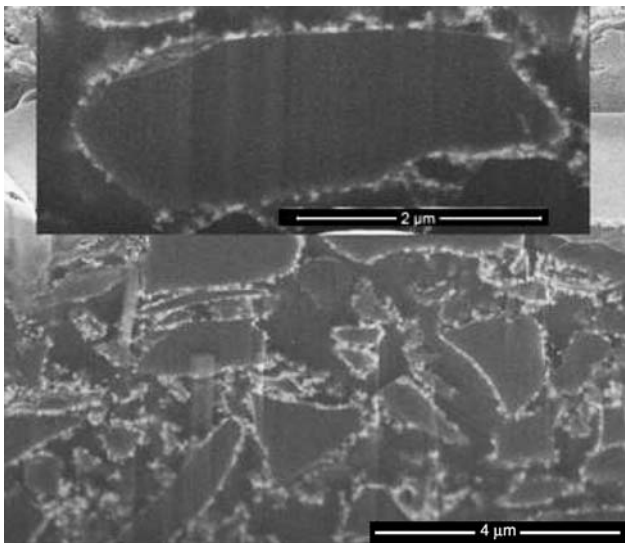

Fig. 11 Cross section SEM micrograph of Ni–B nanolayer coated B_4C particles under the preferred conditions for the three factors studied

B_4C particle with full coverage of the Ni–B nanolayer. The Ni–B nanolayer thickness is less than 55 nm as measured by the field emission electron beam from the focused ion beam microscope. The thicker locations are believed to originate from the Ni–B nodules in the Ni–B nanolayer. The thin locations are likely contributed by the porous locations of the nanolayer. As seen in Fig. 11, some locations might be as thin as single nanometers. This explains why B_4C particles can be detected during the XPS study.

From these observations, it shows that the critical aspect in obtaining uniform and well-defined Ni–B nanolayer is controlling the nanolayer formation kinetics. For the studied B_4C particles, the Ni–B nanolayer surface is not ideally smooth but shows drastic improvement in comparison to the particle morphology reported in many studies. Also, the less than 55 nm thickness Ni–B coating is a substantial improvement from the much thicker coating that has been reported [24, 25]. The small B_4C particles attached onto the micron size B_4C particle surfaces (Fig. 2) could also have contributed to the less than ideal nanolayer morphology. This new particle surface modification capability is expected to make important contributions to improving the processability and performances of B_4C-based materials.

Conclusions

Ni–B nanolayers are coated onto B_4C particles by electroless coating with different amounts of activation agent $PdCl_2$ and complexing agent $C_2H_8N_2$, and different reducing agent $NaBH_4$ addition rates. SEM and XPS results

show that when B_4C:Pd^{2+} ratio is 1:0.005, the nanolayer covers the B_4C particle surfaces with the least roughness. Complexing agent $C_2H_8N_2$ improves the Ni–B nanolayer morphology but lowers its growth rate. When Ni^{2+}:$C_2H_8N_2$ ratio is 1:6, continuous mesh-like nanolayer covers the B_4C particle surfaces. The Ni–B nanolayer formation is also dependent on the rate that Ni^{2+} is reduced. Reducing agent $NaBH_4$ addition rate affects the Ni–B nanolayer thickness and composition. Additional electroless coating study is carried out under the preferred conditions for the above three factors to demonstrate the nanolayer formation capabilities on the B_4C particle surfaces.

Acknowledgement The authors acknowledge the financial support from National Science Foundation under grant No. DMI-0620621.

References

1. Lide DR (2008) CRC handbook of chemistry and physics, 88th edn. CRC Press, Boca Raton, FL, p 12
2. Chen MW, Mccauley JW, Hemker KJ (2003) Science 299:1563. doi:10.1126/science.1080819
3. Jung CH, Lee SJ (2005) Int J Refract Met Hard Mater 23:171
4. Thévenot F (1990) J Eur Ceram Soc 6:205. doi:10.1016/0955–2219(90)90048-K
5. Tom RT, Nair AS, Singh N, Aslam M, Nagendra CL, Philip R, Vijayamohanan K, Pradeep T (2003) Langmuir 19:3439. doi:10.1021/la0266435
6. Bhattacharjee B, Hsu CH, Lu CH, Chang WH (2006) Phys E 33:388. doi:10.1016/j.physe.2006.04.007
7. Elder SH, Cot FM, Su Y, Heald SM, Tyryshkin AM, Bowman MK, Gao Y, Joly AG, Balmer ML, Kolwaite AC, Magrini KA, Blake DM (2000) J Am Chem Soc 122:5138. doi:10.1021/ja992768t
8. Ming M, Chen Y, Katz A (2002) Langmuir 18:8566. doi:10.1021/la026055r
9. Lu Y, Yin YD, Li ZY, Xia YA (2002) Nano Lett 2:785. doi:10.1021/nl025598i
10. Monir Vaghefi SM, Saatchi A, Ebrahimian-Hoseinabadi M (2003) Surf Coat Technol 168:259. doi:10.1016/S0257-8972(02)00926-X
11. Baskaran I, Kumar RS, Narayanan TSNS, Stephen A (2006) Surf Coat Technol 200:6888. doi:10.1016/j.surfcoat.2005.10.013
12. Rao Q-L, Bi G, Lu Q-H, Wang H-W, Fan X-L (2005) Appl Surf Sci 240:28. doi:10.1016/j.apsusc.2004.07.059
13. Oraon B, Majumdar G, Ghosh B (2007) Mater Des 28:2138. doi:10.1016/j.matdes.2006.05.017
14. Ebrahimian-Hosseinabadi M, Azari-Dorcheh K, Moonir Vaghefi SM (2006) Wear 260:123. doi:10.1016/j.wear.2005.01.020
15. Arai S, Endo M, Hashizume S, Shimojima Y (2004) Electrochem Commun 6:1029. doi:10.1016/j.elecom.2004.08.001
16. Ang LM, Hor TSA, Xu GQ, Tung CH, Zhao SP, Wang JLS (1999) Chem Mater 11:2115. doi:10.1021/cm990078i
17. Wang F, Arai S, Park KC, Takeuchi K, Kim YJ, Endo M (2006) Carbon 44:1307. doi:10.1016/j.carbon.2005.12.049
18. Chen YJ, Cao MS, Xu Q, Zhu J (2003) Surf Coat Technol 172:90. doi:10.1016/S0257-8972(03)00320-7
19. Vélez M, Quiñones H, Giampaolo ARD, Lira J, Grigorescu IC (1999) Int J Refract Met Hard Mater 17:99. doi:10.1016/S0263-4368(98)00035-3
20. Zhu XJ, Dong H, Lu K (2008) Surf Coat Technol 202:2927. doi:10.1016/j.surfcoat.2007.10.021
21. Brandow SL, Dressick WJ, Marrian CRK, Chow GM, Calvert JM (1995) J Electrochem Soc 142:2233. doi:10.1149/1.2044280
22. Zhu XJ, Lu K (2006) In Proceeding of 2006 materials science & technology international conference, innovative processing and synthesis of ceramics, glasses and composites, Cincinnati, OH, October, organized by N. P. Bansal and J. P. Singh, p 421
23. Delaunois F, Petitjean JP, Lienard P, Jacob-Duliere M (2000) Surf Coat Technol 124:201. doi:10.1016/S0257-8972(99)00621-0
24. Mondal A, Sabyashachi N, Mondal A, Bandopadhyay S, Gangopadhyay U, Saha H (2004) Mater Res Bull 39:2187. doi:10.1016/j.materresbull.2004.08.002
25. Narayanan T, Seshadri S (2004) J Alloys Compd 365:197. doi:10.1016/S0925-8388(03)00680-7